

# **Auditory nerve first-spike latency and auditory absolute threshold: a computer model.**

Ray Meddis

Centre for the Neural Basis of Hearing at Essex, Department of Psychology,  
University of Essex, Colchester, CO4 3SQ, United Kingdom.

Running Title: Meddis: Computer model of AN first-spike latency

Current Address:  
Department of Psychology,  
University of Essex,  
Colchester, CO4 3SQ, United Kingdom.  
Electronic Mail: rmeddis@essex.ac.uk

Date submitted:

## **Abstract**

A computer model of the auditory periphery was used to address question of what constitutes the physiological substrate of absolute auditory threshold. The model was first evaluated to show that it is consistent with experimental findings that auditory-nerve fiber spikes can be predicted to occur when the running integral of stimulus pressure reaches some critical value (Heil, P. and Neubauer, H., 2001, J. NeuroSci., 15, 7404-7415). It was then modified to examine two possible ways in which the accumulation and dissipation of IHC pre-synaptic calcium might explain this effect. Both methods gave results that matched the animal data. It was also shown how the rate of dissipation of pre-synaptic calcium could be used to explain the origin of differences between low and high-spontaneous rate fiber types. The critical value of the integrated pressure at which spiking occurs is not a parameter of the model but is an emergent property and is higher for low than for high spontaneous-rate fibers. This is also in agreement with the animal data. When spiking activity is aggregated across a number of similar high spontaneous-rate fibers and used as the input to a model of a cochlear nucleus coincidence-neuron, its response can be used to judge whether or not a stimulus is present. A simulated psychophysical experiment was used to demonstrate that this simple decision procedure can reproduce measurements of absolute auditory threshold for tones in quiet where the threshold is a joint function of both time and level.

PACs: 43.64.Bt, 43.64.Ld, 43.66Ba, 43.66Cb

## Introduction

Heil and Neubauer (2001) have presented evidence of long-duration (>100ms) temporal integration in the auditory periphery. Using single-fiber auditory nerve (AN) recordings, they showed that the latency to the first action potential (AP) following the onset of a pure-tone stimulus is a function of both the amplitude and the duration of the stimulus. Specifically, they showed that the time of this first spike following the onset of a pure tone stimulus can be predicted using the integral of the sound pressure envelope of the stimulus at the time when the first spike occurred. The principle is illustrated in Figure 1 for two 30 dB SPL tones, where the two tones have different onset ramps (dotted lines). The two integrals of the sound pressure envelopes (smooth lines) rise until a critical value,  $T_c$ , is reached. At this point a spike event is predicted to occur in the AN fiber.

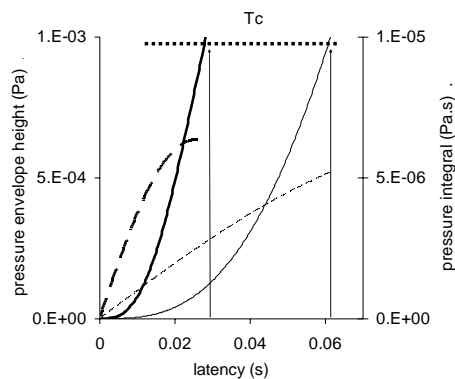


**Figure 1. General scheme of pressure integration paradigm. Dotted lines show two stimulus ramps (pressure: left ordinate). Smooth lines show the integral of stimulus pressure (pressure\*time: right ordinate) for the two ramps. Predicted latency is the time,  $L$ , at which the integral of the pressure exceeds a critical threshold value,  $T_c$ .**

This simple picture is complicated by the presence of spontaneous activity and by the observation that different fibers initiate a first spike at different values of  $T_c$ . Spontaneous activity can be discounted using statistical techniques but  $T_c$  has been shown to be systematically related to fiber type. Low spontaneous-rate (LSR) fibers were found to initiate spiking activity at higher levels of integrated pressure than high spontaneous rate (HSR) fibers. Heil and Neubauer reasoned that the integration of stimulus pressure must occur at the inner hair cell (IHC) / AN synapse; after the receptor potential but before the release of transmitter. During acoustic stimulation, the receptor potential is raised and calcium enters the pre-synaptic region of the IHC where it facilitates the release of transmitter. They propose that the accumulation of calcium is the physiological analogue of the integration of sound pressure.

Calcium, however, is rapidly cleared from the synapse by chemical buffering. This makes the accumulation of calcium a 'leaky integrator'. It is a common belief that a

leaky integrator with a short decay time constant can only integrate over short periods of time. This is, however, a misperception. The time taken for a physical integrator to reach some critical value is primarily a function of the rate of inflow into the system, whether the integrator is leaky or not. A fast rate of discharge simply *increases* the time taken to reach a threshold. Heil and Neubauer appreciated this fact. They distinguished between the rate of influx of calcium and the time constant of the calcium clearance process and hypothesised that either or both might explain the difference between HSR and LSR fibers. The relative merits of these two hypotheses are evaluated in computer-modelling project described below.

While their conjecture is interesting purely in terms of its implications for auditory physiology, it might have much wider implications for understanding the psychophysical phenomenon of temporal integration at absolute threshold; the phenomenon where the absolute perceptual threshold for a tone presented in silence is lower if the stimulus is longer (see Eddins and Green, 1995 for a review). Heil and Neubauer have gone on to show that single-unit activity in the auditory cortex shows the same latency effect as that observed in single-fiber activity in the AN. They have also shown parallels with psychophysical data in a number of mammalian species including human listeners. Psychophysical temporal integration, therefore, with its long integration times (up to 500 ms) might be explained, at least in part, by pre-synaptic activity in the IHC.

However, the argument is incomplete because first-spike latency is not the same thing as threshold. Latency measurements require a knowledge of the time of onset of the signal and, by definition, this is not available to the nervous system prior to the detection of that signal. Moreover, there is the problem of how a single AN AP driven by a stimulus can be distinguished from a spontaneously generated AP. The final section of this report will propose a physiologically plausible system for converting first-spike latency effects into threshold phenomena by modelling single units in the cochlear nucleus.

A number of previous studies in mammals (e.g. Clock et al., 1998; Gersuni, 1965; Viemeister et al., 1992) have shown that thresholds based on AN spike counts show the same trading relationship between stimulus level and duration as found in psychophysical studies. These studies are consistent with the first-spike latency data but they do not determine the *location* of the temporal integrator. The use of spike counts in these studies implies that an integration window (where the counting takes place) is located *after* the AN. Moreover, the detailed protocol used by these spike count studies normally assumes that the detection system already knows when to start and stop counting, i.e. when the stimulus begins and ends. This is another process that can only be regulated by more central mechanisms. By contrast Heil and Neubauer propose that the integrator occurs *before* the AN and does its own counting by accumulating calcium ions. While it is possible that there is more than one integrator, this study will focus on the explanatory power of their idea that the main integrator is located peripherally in the cochlea.

Clock et al. (1993) studied single unit thresholds of primary-like and chopper neurons in the cochlear nucleus and showed that threshold declined with signal duration at least up to 128-ms. The modelling study will also simulate their result in that it

explores a possible process whereby AN first-spike latency effects influence thresholds in CN units.

The computer model to be used is based on an existing model of the auditory periphery (Sumner et al., 2002a & b, 2003, Holmes et al. 2004, Meddis and O'Mard, 2005) followed by an extension to include a simulation of a CN chopper neuron based on another existing model (Hewitt and Meddis, 1993, 1994; Wiegrebe and Meddis, 2004). The peripheral model is suited to our purpose because it already incorporates a 'leaky integrator' approach to pre-synaptic calcium dynamics. In the study it will be modified to allow simulation of both hypotheses (rate of influx *versus* rate of dissipation) concerning the role of calcium mechanisms in explaining the differences between LSR and HSR AN fibers.

Only one other relevant modelling study has been published (Krishna, 2001). He used a more schematic computer model successfully to simulate first-spike latency data. The model was successful because it included an explicit 'integration module' with a critical threshold function. Although the model is physiologically inspired, this integration module was not associated with any specific physiological function except that the author explicitly *ruled out* the possibility that it could be calcium dynamics. This rejection was based on the grounds that the time constants of calcium dynamics were too short. The following study will show that this widely-held objection is not well founded. Indeed the rapid dynamics of pre-synaptic calcium are ideally suited to the long time scales of first-spike latency effect.

## **Computer model**

The input to the computer model of the auditory periphery is an arbitrary acoustic stimulus. Its output is a stream of spiking events in one or more parallel AN fibers all innervating the same location on the cochlear partition. The complete peripheral model consists of a cascade of five stages estimating: (1) stapes velocity, (2) BM velocity, (3) IHC receptor potential, (4) IHC pre-synaptic calcium currents, (5) transmitter release events at the IHC-AN synapse, and (6) AN spiking response including refractory effects. The output of the peripheral model is used as input to a second model of a single cochlear nucleus chopper neuron.

A complete description of the model equations and parameters is given in the appendix. Except where specified all equations and parameters are exactly as specified in the most recent previously published evaluations of the component modules. The model was implemented using routines from a library of C-code modules in the Development System for Auditory Modelling (DSAM) which is published by Essex University. The full model of the auditory periphery was implemented as a programme sequence using the Auditory Modelling System (AMS) application<sup>1</sup>. The MATLAB programming language was used to create the sequence of stimuli, to initiate a model run and to collect, analyse and display the results. The model was evaluated at a sampling rate of 100 kHz.

### ***Pre-synaptic calcium***

Two models of calcium dynamics are evaluated below. The first model (Sumner model) identifies the difference between fiber types in terms of the different rates of influx of calcium into the cell and assumes that LSR fibers have the lowest rate of calcium influx for a given receptor potential. The second model (calcium clearance

model) assumes a fixed rate of influx for all fiber types but defines the differences among fibers in terms of the rate at which calcium is cleared from the synapse. LSR fibers, for example) have the fastest rate of clearance or pre-synaptic calcium.

*Sumner model.* Calcium concentration  $[Ca^{2+}](t)$  is modeled as a first-order low-pass filtered function of the trans-membrane calcium current,  $I_{Ca}(t)$

$$\frac{d[Ca^{2+}](t)}{dt} = [I_{Ca}(t) - [Ca^{2+}](t)] / \tau_{Ca} \quad (1)$$

where  $\tau_{Ca}$  is the time constant of calcium clearance and

$$I_{Ca}(t) = G_{Ca}^{\max} m_{I_{Ca}}^3(t) (V(t) - E_{Ca}) \quad (2)$$

where  $V(t)$  is the receptor potential,  $E_{Ca}$  is the reversal potential for calcium and  $G_{Ca}^{\max}$  is the maximum calcium conductance in the vicinity of the synapse,  $m_{I_{Ca}}(t)$  is the fraction of calcium channels that are open (see appendix for the determination of  $m$ ). The probability that an available transmitter vesicle will be released into the synaptic cleft is proportional to the cube of the  $Ca^{2+}$  concentration:

$$k(t) = \max([Ca^{2+}]^3(t) - [Ca^{2+}]_{thr}^3, 0) \quad (3)$$

Where  $z$  is a scalar and  $[Ca^{2+}]_{thr}^3$  is a threshold parameter. Both  $G_{Ca}^{\max}$  and  $[Ca^{2+}]_{thr}^3$  are also typically changed when modeling the difference between LSR and HSR fibers.

*Calcium clearance hypothesis.* Evaluation 2 investigates Heil and Neubauer's idea that differences between fiber types might be explained in terms of differences in the rate of calcium dissipation. The conversion of the model to implement this idea requires only two small changes.

First, equation (1) is simplified so that the time constant of dissipation of calcium,  $\tau_{Ca}$ , is applied only to the accumulated calcium and not to the calcium influx.

$$\frac{d[Ca^{2+}](t)}{dt} = I_{Ca}(t) - [Ca^{2+}](t) / \tau_{Ca} \quad (4)$$

Second, equation (3) is simplified to remove the threshold parameter,  $[Ca^{2+}]_{thr}^3$ .

$$k(t) = zCa^3(t) \quad (5)$$

## Evaluation 1: Sumner model

Heil and Neubauer (2001, 2003) measured the 'latency to first spike' of single AN fibers in cat in response to pure tones. Both the level of the tones and the steepness of the onset ramp were varied. The following demonstration replicates their experimental procedure in detail using the computer model of the guinea pig periphery. Model parameters were unchanged from (Sumner et al., 2002a & b, 2003)

but incorporated small changes described in Meddis and O'Mard (2005). All parameters are given in the appendix.

Pure-tone stimuli (200 ms) were shaped with cosine-squared rise and fall functions with 7 different rise times equally spaced on a log scale between 1.7 and 170 ms. They were presented at levels that varied between 0 and 90 dB SPL in 10 dB steps. Each stimulus was presented 20 times and the mean latency to first spike was measured for each of the 70 stimuli. Latencies were measured between the beginning of the stimulus onset ramp and the first spike to occur after that time. If no spike occurred before the end of any stimulus on any of the 20 trials, the mean latency for that combination of level and ramp duration was treated as indeterminate. Each trial began with a 50-ms period of silence which was used to assess the spontaneous firing rate. Figure 2 (top row) shows model first-spike latencies measured as a function of both level and ramp duration.

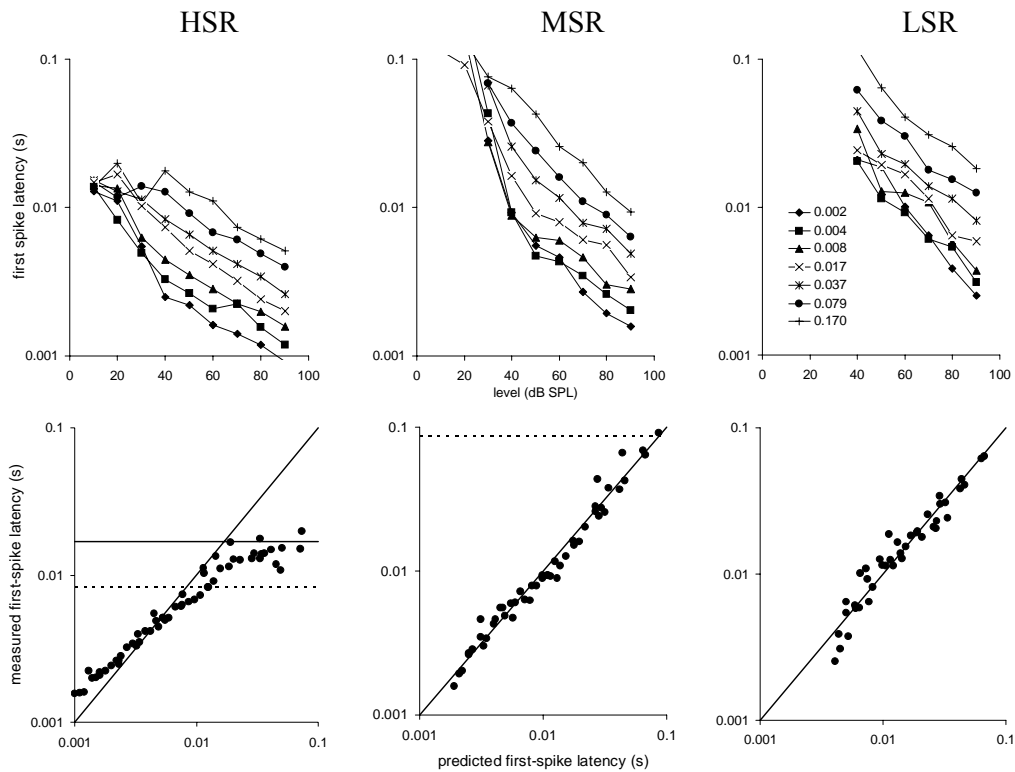


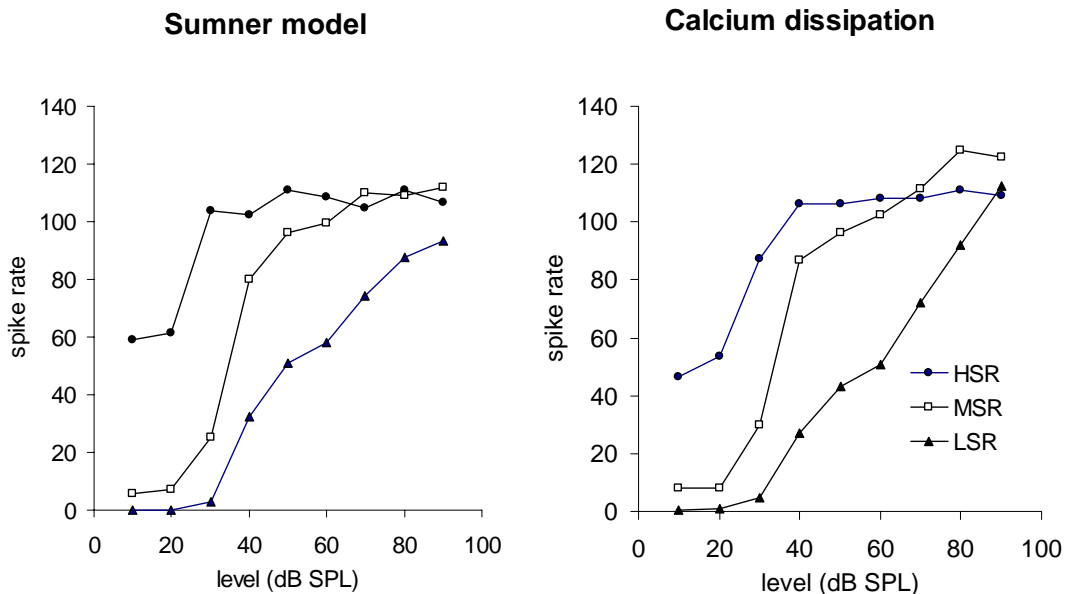
**Figure 2. Model AN first-spike latencies using the Sumner model for HSR, MSR and LSR fiber types. Top row: first spike latencies as a function of tone level (x-axis) and onset ramp duration (separate functions). Bottom row: first spike latencies as a function of predicted latencies using the prediction function  $L_{pred}=L_{min} + L_c$  (see text). Horizontal continuous lines are ‘expected latency’ ( $1/\text{spontaneous rate}$ ). Horizontal dotted lines indicate the cut-off criterion for omitting data from the best-fit analysis for the prediction function. The best fit values for  $L_{min}$  are 1, 2 and 3 ms for HSR, MSR and LSR fibers respectively. The corresponding values for  $T_c$  are  $5.3e-6$ ,  $1.7e-5$  and  $1e-4$  Pa.s.**

The mean latencies ( $L$ ) for the animal data could be predicted by the sum of two quantities;  $L_{\min}$  and  $L_c$ , where  $L_{\min}$  is a minimum latency common to all measurements for that fiber and  $L_c$  is the delay before the integral of the pressure envelope reaches a critical threshold value  $T_c$  (measured in Pascals.sec). These two free parameters,  $L_{\min}$  and  $T_c$  were estimated by finding the least-squares, best fit between the logarithms of the predicted and actual latencies (see Heil and Neubauer, 2001, for a full account of the relevant procedures and justification). Measured latencies were used in the calculations only if these were shorter than half the average interval between spikes during spontaneous activity. Figure 2 (bottom row) plots the actual latencies against the predicted latencies as a function of tone level and ramp duration.

High (HSR), medium (MSR) and low(LSR) spontaneous-rate model fibers all show the expected effect and the plots are virtually identical with those given by Heil and Neubauer (2001 Figs 2B, 5 A-D, 6 A & C). The small deviations from the predicted line (diagonal) for short and long predicted latencies are also a characteristic of the animal data (Heil and Neubauer, 2001, Fig. 6 A & C) and are not a shortcoming of the model. These deviations reflect the fact that the calcium integration system is 'leaky' and, as a consequence, is not a perfect integrator of stimulus pressure. Heil and Neubauer (2001, Fig. 8D) obtained critical threshold integrals ( $T_c$ ) in the region  $1e-7$  to  $1e-4$  Pa.s. The values shown in Fig. 2 are comfortably within that region. They also found that  $T_c$  was greater for LSR than HSR fibers. This was also true of the model data.

## Evaluation 2: Calcium dissipation model

Heil and Neubauer speculated that the rate of dissipation of calcium from the pre-synaptic region might also be a critical parameter determining first spike latency; that the variation in spontaneous rate across nerve fibers might be explained in terms of differences in the rate of calcium clearance. In the Sumner model, the rate of calcium influx time varies across fiber types while the calcium clearance time constant ( $\tau_{Ca}$ ) is fixed. To test the new hypothesis (that influx is fixed while  $\tau_{Ca}$  varies across fiber types), small changes to the Sumner model were made as described above.



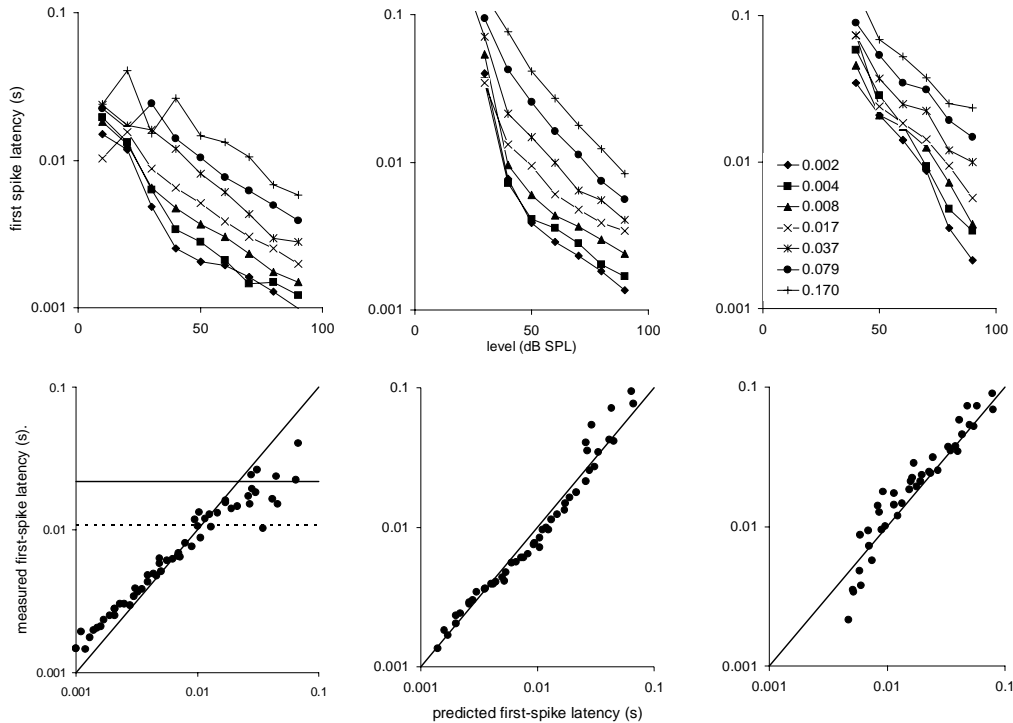
**Figure 3. Rate level functions for the original and modified Sumner models. Rate is based on the all the spikes during presentation of a 200-ms pure tone presented at BF (4 kHz). Tones had a 17-ms cosine-squared onset ramp. In the revised model,  $\tau_{Ca}$  values were 0.35, 0.15 and 0.075 ms for HSR, MSR and LSR fibers respectively.**

Figure 3 shows the rate-level function for both the original Sumner model and the calcium clearance version of the model. The results show that both models give a useful account of the differences between fiber types as observed in laboratory studies. HSR fibers have higher spontaneous rates, a lower rate-threshold and a lower saturation-threshold than LSR fibers. The differences in the shape of the rate-intensity functions are similar to the differences observed between LSR and HSR fibers in mammalian physiological studies (Liberman and Kiang, 1978; Winter et al., 1990).

HSR

MSR

LSR



**Figure 4. Model first-spike latency using the modified (calcium clearance) model for HSR, MSR and LSR fiber types. (See Fig. 2 for explanation). The best fit values for  $L_{min}$  are 1, 1 and 6 ms for HSR, MSR and LSR fibers respectively. The corresponding values for  $T_c$  are  $5.3e-6$ ,  $1.7e-5$  and  $1e-4$  Pa.s.**

First-spike latency data for the same three fiber types are shown in Fig. 4. Once again, the critical pressure integral required to fit the response of the modified model lies within the range observed by Heil and Neubauer and the critical pressure integral,  $T_c$ , increases across the HSR-LSR spectrum. In conclusion, both the Sumner calcium-influx model and the new calcium-clearance model are able to simulate the first spike latency effect and are, therefore, both candidate explanations in terms of pre-synaptic calcium dynamics.

The central difference between the two models is, of course, an empirical issue. The question as to whether the low spontaneous firing rate of LSR fibers is caused by different rates of dissipation or different rates of calcium influx into the cells is more properly decided by further laboratory observation. In evaluations 3 and 4 below, both models were tested and gave approximately the same results. The illustrations however, use only the calcium-clearance model to avoid unnecessary duplication.

For both models, it should also be noted that the critical threshold integral,  $T_c$ , as estimated from the first-spike latencies, is not a parameter of the model but an emergent property. When the pre-synaptic calcium level rises, the probability of release of a transmitter vesicle rises as a function of the third power of the calcium level. As a consequence, the probability of a release event increases very rapidly. However, there is no ‘trigger’ calcium threshold, *per se*, in the model, only the *appearance* of one.

### Evaluation 3: Coincidence detection

The first-spike latency data provide evidence that temporal integration of a kind is taking place at an early stage in the auditory system. The integration takes place over relatively long time periods (more than 100 ms for LSR fibers). This suggests that the first-spike latency might be related to the temporal integration observed in psychophysical studies. However, it is not immediately obvious how first-spike latency effects can be linked to threshold detection decisions. One possibility is that the nervous system fails to detect low-intensity, short sounds because the time taken to accumulate enough pre-synaptic calcium to initiate a spike is greater than the duration of the signal. If the signal is too weak or too short, no spike is initiated before the end of the signal and no detection occurs.

The weakness of this idea is that detections cannot be based on single APs. Most AN fibers are spontaneously active and many spikes will occur during the presentation of even a sub-threshold stimulus. There is no simple way of discriminating between a spontaneous spike and stimulus-driven spike in a single fiber. It is true that some LSR fibers show little or no spontaneous activity and any one of their spikes is highly likely to be stimulus-driven. However, LSR fibers cannot be used, in isolation, to explain psychophysical threshold because their rate thresholds are typically higher than those of HSR fibers. The latter are, therefore, the natural candidates for determining psychophysical absolute threshold.

One solution to the problem of spontaneous events is to use only coincidental activity across a number of fibers as an indicator of the presence of a physical stimulus. During spontaneous activity, spikes in different fibers occur at random with respect to one another and coincidental spikes are rare. When a stimulus is present, APs are more likely to be synchronised to features of the stimulus such as stimulus onset with the result that fibers are more likely to fire coincidentally. This approach has been used in a previous study where coincidental activity was used to predict absolute psychophysical thresholds in a forward masking paradigm (Meddis and O'Mard, 2005).

The model to be evaluated below feeds the output of 20 HSR AN fibers into a coincidence-detector neuron. This consists of two stages; a low pass filter to simulate dendritic smoothing followed by a simple computer model of the neuron soma (McGregor, 1987) described in the appendix and elsewhere (Hewitt and Meddis, 1993; Wiegrebe and Meddis, 2004). The dendritic filter has a low pass cut off of 200 Hz which equates to a time constant of approximately 0.7 ms. As a result, the CN unit responds only when the input fibers generates spikes very close together in time. This is roughly equivalent to a previous implementation (Meddis and O'Mard 2005) where the inputs were simply aggregated into 0.5 ms bins and a minimum count criterion applied.

In this evaluation, the protocol of stimulus presentation is exactly the same as that used in evaluations 1 and 2 except that latency is based on the first spike produced by the CN neuron. The results are shown in Fig. 5 where the diagonal line shows the predicted latency estimated using the same procedure used with AN fibers above. The coincidence latencies are a good fit to the prediction and the correspondence between predicted and actual latencies shows a greatly extended temporal range. For HSR AN fibers the relationship between first-spike latency and pressure integral is

valid only up to approximately 10 ms (see Fig.4). This is because the spontaneous activity of the fiber introduces an upper limit to the length of intervals occurring between successive spikes. When we use the coincidence criterion, this limitation is removed because the coincidence neuron does not respond to spontaneous AN spikes. The figure shows that the relationship remains valid up to at least 100 ms.

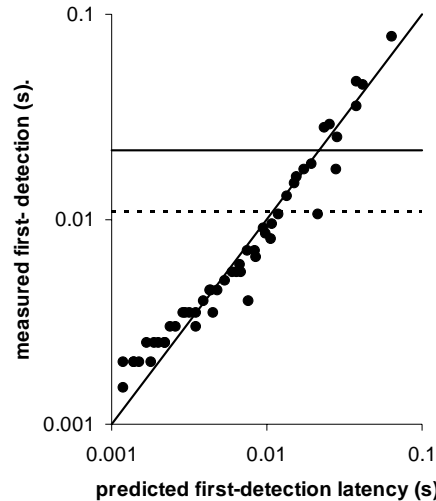


**Figure 5. First-spike latency of a model coincidence neuron plotted against predicted first-spike latency. The neuron receives input from 20 model HSR fibers. Horizontal continuous lines are ‘expected latency’ (1/spontaneous rate) of the CN unit. Horizontal dotted lines indicate the cut-off criterion for omitting data from the best-fit analysis for the prediction function. Evaluation 4: CN and Psychophysical thresholds**

The results obtained in evaluation 3 suggest that the coincidence detection model might be capable of temporal integration over much longer time-scales that parallel those observed using a *psychophysical* paradigm. A low-intensity stimulus will produce a coincidence event with a long latency. If that stimulus is short, the coincidence event will not occur before its termination. As a result the length of the signal will be critical in determining whether it is detected at all. To evaluate this possibility, the absolute threshold of the model was measured as a function of stimulus duration. The procedure was based as closely as possible on a psychophysical experiment described by Florentine et al. (1988).

Clock et al. (1993) measured the responses of CN units using a similar paradigm. We can assess the effectiveness of the computer model by comparing its results with their data. There is however, one complication. Clock et al. found that the threshold for their CN unit declined with duration up to 128 ms but the function levelled out for longer durations. This does not agree with the human data that is normally interpreted to indicate a continued decline in threshold at least up to 500 ms. Clock et al. drew attention to statistical complications associated with their method of counting CN unit spikes. They assumed that the decision was made by an ‘ideal observer’ with complete knowledge of the time of the onset and offset of the stimulus so that probe-spike counts were restricted to the time that the probe was on. In the experiment with human listeners, the stimuli (irrespective of their length) were presented during a 500-ms inspection window. If all spikes within that window are counted, the statistical

nature of the decision changes. Both approaches ('probe count' and 'window count' respectively) will be considered below.

Absolute thresholds were measured using a two-interval, two-alternative, forced-choice paradigm. On each trial, two independent 550-ms observation intervals were used; one silent interval and one containing a probe tone presented centrally in the observation window. The model's task was to use the output of the coincidence detection neuron to choose which interval contained the stimulus. Threshold measurements were made using a one-up, two-down adaptive procedure which converges on the signal level yielding 70.7% correct responses (Levitt, 1971). The probe level started at 50 dB SPL and was reduced by steps of 5 dB until the first reversal after which the step size was reduced to 2 dB. Thresholds were calculated using the average level of the last two reversals. Stimuli were pure tones presented at BF (4 kHz) with rise times of 1 ms. Separate threshold estimates were made for signal durations of 2, 4, 8, 16, 32, 64, 128, 256, and 512 ms.

For each of the two observation intervals, the model made an independent decision as to whether a stimulus was or was not present. A 'yes' decision was made if the neuron generated *at least one spike* during the counting period. Separate decisions were made for the stimulus and control condition. If only one interval generated a 'yes' response, that interval was chosen. If both intervals generated a 'yes' decision, the model chose the interval with the larger number of spikes (or selected one at random in the case of a tie). If no detection occurred in either interval, the model chose one of the two alternatives at random. In the example below, the spontaneous rate of the CN neuron was very low (<2 spikes/s). Near threshold, the spike count was typically zero or one.

The model was exactly the same as that described in evaluation 3. Figure 6A shows absolute threshold as a function of signal duration based on both methods of calculating spike counts (see above). All but one of the thresholds are below the compression threshold for the basilar membrane simulation (horizontal dotted line). Threshold decreases monotonically between 2 and 512 ms. The two datasets are similar except at very short durations.

Figure 6B compares the same data with the psychophysical thresholds of Florentine et al. (1988, Fig. 1; mean of 5 listeners) and the physiological measurements of Clock et al. (1993) based on single unit measurements in the CN. The model data have been shifted so that they are close to the human data in the mid-duration range. The model data fit the human data reasonably well up to 64 ms but have higher shifted thresholds for longer durations. Both the model and the human data have roughly level functions at very long durations. However, the levelling begins earlier for the model data. At very short durations, the probe spike count yields a better match to the human data than the window spike count. The model and the human data all show a steeper function at the shortest durations and this may be caused by basilar compression affecting some of the observations contributing to the threshold computations.

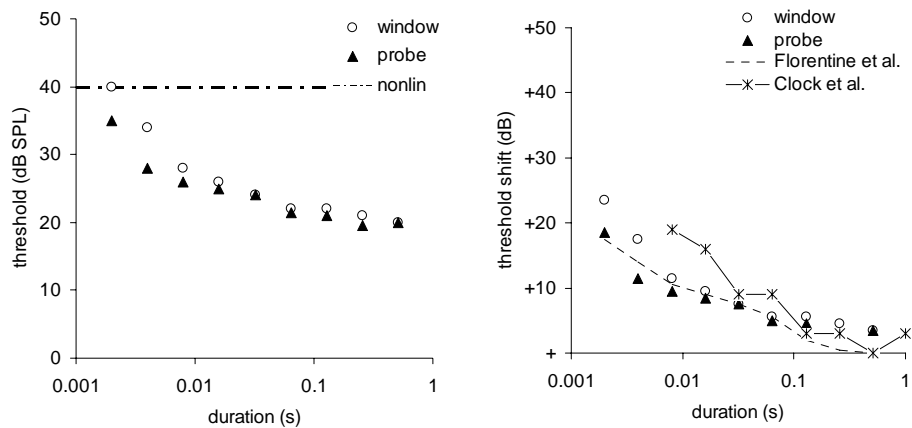


**Figure 6. A: Absolute threshold of a model cochlear nucleus coincidence neuron as a function of signal duration. Thresholds are based on total spike counts in the 500-ms observation window (open circles) or exclusively when the probe was playing (filled triangles). Each threshold is the mean of 20 trials. Signals are BF (4-kHz) tones. The horizontal dotted line indicates the level at which basilar membrane compression begins in the basilar membrane stage of the model.**

**B: Threshold shift representation of the same data. Also shown are human data (Florentine et al., 1988; dashed line) and animal CN unit thresholds (Clock et al., 1993) both shifted to give 0 dB shift at the longest duration. The model data are shifted so that the middle durations approximately match the human data.**

Clock et al. speculated that the spike counts based on the probe period alone might be subject to a statistical artefact. They measured the mean (M) and standard deviation (SD) statistics of spike counts and found that the ratio SD/M decreased with duration up to 128 ms and then levelled out at long durations. This means that an 'ideal observer' who takes advantage of knowledge of the time of occurrence of the probe should show an improved ability to distinguish between signal and noise only up to 128 ms. This complication should not apply if the counting window duration is fixed. Notwithstanding their argument, no difference was found between the two methods in this study at long durations. If any difference is present, it occurs at short durations. The best fit to human data at short durations is obtained using the probe spike count. If this correspondence were to be shown to be true in general it would imply that the human observer is taking advantage of knowledge of the expected time and duration of delivery of the probe during the observation window.

## Discussion

Evaluation 1 showed that an existing model of IHC synapse function can simulate the basic first-spike latency findings of Heil and Neubauer (2001) The model first-spike latency could be predicted on the basis of the integral of the stimulus pressure envelope between the onset of the tone stimulus and the time of the first spike. The pressure integral ( $T_c$ ) at which the first spike typically occurred was lower for HSR than LSR fibers. This is also in agreement with the animal data. The model latencies can be attributed to the accumulation of pre-synaptic calcium during tone presentation. The effect was shown to operate at least up to tone durations of 200 ms.

Evaluation 2 modified the model so that fiber type was controlled using the rate of clearance of calcium from the pre-synaptic region. This model generated realistic rate-level functions for the different fiber types and was also able to simulate the first-spike latency data. In terms of performance, there was little to distinguish the two models. However, the modified model gave a simpler account of the IHC calcium dynamics and dispensed with the use of a specific threshold parameter. As a consequence, it is easier to see that the threshold differences between the fiber types are emergent properties rather than fixed properties of the model. In general terms, the modelling work supports the conjecture of Heil and Neubauer that first-spike latency is determined by the accumulation of pre-synaptic calcium but it does not help decide whether these differences are caused by different rates of calcium influx or clearance. It does show that both possibilities are worthy of further investigation. The rate of calcium integration offers a potentially useful explanation of the prominent differences among AN fiber types. LSR fibers, for example, require a higher integrated pressure before the first spike event. This suggests that calcium integrates more slowly for these fibers. This could be either because calcium is entering the pre-synaptic site more slowly or because it dissipates more efficiently. The modelling work suggests that either explanation is viable.

Evaluation 3 linked first-spike latency with absolute perceptual threshold, by extending the model to include a CN coincidence neuron whose input was 20 HSR fibers. The neuron was tuned to be all but unresponsive to the uncorrelated spontaneous activity of the input fibers but responsive to correlated stimulus-driven activity. CN latencies also showed a strong relationship to integrated pressure. However, this relationship held at longer stimulus durations in the CN model than with the AN HSR fiber model. HSR fibers have spontaneous activity which obscures this relationship when the latencies are longer than approximately half of the spontaneous latency ( $1/\text{spontaneous rate}$ ). This limits the validity of the link beyond 10 ms. The CN coincidence unit is not subject to this restriction because it ignores AN spontaneous activity and responds only to signal driven AN events. A relationship to integrated pressure was visible up to 100 ms in this test.

Evaluation 4 explored a possible link between AN first-spike latency and absolute perceptual threshold by simulating a psychophysical experiment (Florentine et al. 1988) but substituting the model CN unit for the human listener. The model data were similar in number of respects to the human data. While the meaning of the correspondence can easily be overstated, it is clear that, in principle at least, that a coincidence detecting neuron receiving input from similar HSR fibers does show temporal integration up to 500 ms. The slope of the threshold-duration function is, however, less steep than the psychophysical data after 64 ms. The modelling result is similar to the results of Clock et al. (1993). It is a common view that temporal integration must take place relatively late in the auditory processing sequence because the long duration of the integration period contrasts with the short time constants typically found in peripheral physiological processes. However, this is clearly based on a misunderstanding because 'leaky integrator' systems with short time constants are indeed capable of charging very slowly if the input current is low enough.

A striking counter example to the hypothesis modelled here is the finding of Gerken (1979) that the behavioural threshold in cat for brief electrical pulses delivered to electrodes in the CN of a cat decreased by 7.6 dB per ten-fold increase in the number

of pulses. If this involves the same mechanism as psychophysical auditory temporal integration then it would firmly locate the integration mechanism *after* the IHC/AN synapse and the relationship between first-spike latency and integrated pressure could be seen as irrelevant. Unfortunately the pulse data are open to a range of interpretations. One is that each threshold level pulse (taken as a separate entity) is associated with a small probability of eliciting a detection. As the number of pulses is increased, the probability of at least one of them being detected necessarily increases as well. Using this simple scenario, we might expect a 3 dB reduction in threshold for each doubling of the number of pulses if the probability of detection were linearly related to stimulation level; a figure that is close to the data. Accordingly, any interpretation in terms of integration of the pulse energy across widely spaced pulses should be treated with caution even though that interpretation fits the data just as well.

Another problem concerns the fact that thresholds in this study were based partly on spike counts and the need for counts could imply that more temporal integration is taking place after the CN. However, this is not necessarily the case because, near threshold, the model spike count was typically one or zero because the spontaneous rate of the unit was less than 2 spikes/s. Even if the CN units were more active in silence, another layer of coincidence detection, might be enough to determine thresholds without any further spike counting or temporal integration process. This second coincidence detection stage might be in the inferior colliculus for chopper units for example. These high-order units would respond only when the CN units fired at the same time, i.e. when stimulus driven.

The model study should not be read to imply that the activity of a single coincidence unit in the cochlear nucleus offers an explanation of temporal integration in its many psychophysical guises. There is more to temporal integration than detecting pure tones in silence (Eddins and Green, 1995) and considerably more modelling research would be required to decide on how general the present explanation will prove to be. Moreover, many neurons are likely to be involved in threshold decisions in a real animal and their location and type remain to be defined. However, the modelling study shows that calcium dynamics are a viable explanation of how first-spike latency effects might come about and indicates a possible route for converting these effects into threshold decisions. Further modelling work is required to see if the principle can be extended to explain other aspects of temporal integration. The study also shows that the computer model of the auditory periphery described above could prove to be an adequate vehicle for this purpose.

Eventually, empirical methods will decide the questions of what mechanisms underpin first-spike latency and psychophysical temporal integration. However, the model also investigates the conceptual issue of what constitutes the physiological substrate of absolute auditory threshold. The conventional view (although rarely explicitly stated) equates it with the rate threshold of single HSR fibers whose best frequency is the close to the strongest component frequency of the stimulus. Auditory temporal integration challenges this simplistic approach by insisting that time is a also conceptual component. However, the problem is further complicated by the presence of spontaneous activity in the nerve fiber. A short 2-ms tone burst will not induce more than one AP in a single fiber. There is no way that this single AP can be distinguished from a spontaneously generated AP and yet this stimulus can be detected on a single trial. The model evaluated here presents one solution to this

problem; that units in the cochlear nucleus respond only when multiple AN fibers fire in synchrony. Threshold is then defined in terms of APs in the cochlear nucleus. In this respect, it is convenient for the model that the temporal integration component has already taken place in the IHC/AN synapse and, as a consequence, the level at which sound induces a response in at least one CN unit is a function of both time and level.

## Acknowledgements

This manuscript and the modelling has benefited substantially from the challenging and insightful comments of Brian Moore, Peter Heil and Heinrich Neubauer on a much earlier version of this manuscript. Lowel O'Mard contributed valuable computational support throughout.

## References

- \*Clock, A.E., Salvi, R.J., Wang, J., Powers, and N.L. (1998). "Threshold-duration functions of chinchilla auditory nerve fibers," *Hear. Res.* 119, 135-141.
- \*Clock, A. E, Salvi, R.J., Saunders SS, Powers, N.L. (1993) "Neural correlates of temporal integration in the cochlear nucleus of the chinchilla.," *Hear Res.* 71, 37-50.
- \*Eddins, D.A. and Green, D.M. (1995). "Temporal integration and temporal resolution". In: Moore, B.C.J. (Ed), *Hearing*. Academic Press, San Diego, CA, pp 207-242.
- \*Florentine, M, Fastl, H. and Buus, S. (1988). "Temporal integration in normal hearing, cochlear impairment, and impairment simulated by masking," *J. Acoust. Soc. Am.* 84, 195-203.
- \*Gerken, G.M. (1979) Temporal summation of pulsate brain stimulation in normal and deafened cats. *J. Acoust. Soc. Am.* 66, 728-734.
- \*Gersuni, G.V., 1965. Organization of afferent flow and the process of external signal discrimination. *Neuropsychologia*, 3, 95-109.
- \*Heil, P. and Neubauer, H. (2001). "Temporal integration of sound pressure determines thresholds of auditory nerve fibers," *J. NeuroSci.*, 15, 7404-7415.
- \*Heil, P. and Neubauer, H. (2003). "A unifying basis of auditory thresholds based on temporal summation," *Proc. Nat. Acad. Sci.*, 100, 6151-6156.
- \*Hewitt, M. J. and Meddis, R. (1991). "An evaluation of eight computer models of mammalian inner hair-cell function," *J. Acoust. soc.Am.* 90, 904-917.
- \*Hewitt, M. J. and Meddis, R. (1993). "Regularity of Cochlear Nucleus Stellate Cells: A Computational Modelling Study," *Journal of the Acoustical Society of America* 93, 3390-3399.
- \*Hewitt, M. J. and Meddis, R. (1994). "A Computer Model of Amplitude-Modulation Sensitivity of Single Units in the Inferior Colliculus," *Journal of the Acoustical Society of America* 95, 2145-2159.
- \*Holmes, S., Sumner, C., O'Mard, L. P. and Meddis, R. (2004). 'The temporal representation of speech in a nonlinear model of the guinea pig cochlea' *Journal of the Acoustical Society of America* 116, 3534-3545.
- \*Krishna, B. S. (2002). "A unified mechanism for spontaneous-rate and first-spike timing in the auditory nerve," *J. Comp. Neurosci.*, 13, 71-91.
- \*Levitt, H. (1971). "Transformed up and down methods in psychology," *J. Acoust. Soc. Am.*; 49, 467-477.

- \*Lieberman, M.C., and Kiang, N.Y.S. (1978) "Acoustic trauma in cats. Cochlear pathology and auditory-nerve activity", *Acta Otolaryngol Suppl Supplement*, 358, AN Activity.
- \*Lopez-Poveda, E. A. and Meddis, R. (2001). "A human nonlinear cochlear filterbank," *J. Acoust. soc.Am.* 110 (6): 3107-3118.
- \*MacGregor R.J. (1987). "Neural and brain Modelling", (Academic, San Diego)
- \*Meddis, R. (1986). "Simulation of Mechanical to Neural Transduction in the Auditory Receptor," *J. Acoust. soc.Am.* 79, 702-711.
- \*Meddis, R. (1988). " Simulation of Mechanical to Neural Transduction: Further Studies," *J. Acoust. soc.Am.* 83, 1056-1063.
- \*Meddis, R., Hewitt, M. J. and Shackleton, T. (1990). "Implementation details of a computational model of the inner hair-cell/auditory-nerve synapse," *J. Acoust. soc.Am.* 87, 1813-1818.
- \*Meddis, R., O'Mard, L.P. and Lopez-Poveda, E.A. (2001) "A computational algorithm for computing nonlinear auditory frequency selectivity," *J. Acoust. soc.Am.* 109, 2852-2861.
- \*Sumner, C., Lopez-Poveda, E.A., O'Mard, L.P. and Meddis, R. (2002a). "Adaptation in a revised inner-hair cell model," *J. Acoust. Soc.Am.* 113, 893-901.
- \*Sumner, C., O'Mard, L.P., Lopez-Poveda, E.A., and Meddis, R. (2003). 'A non-linear filter-bank model of the guinea-pig cochlea,' *Journal of Acoustical Society of America* 113, 3264-3274..
- \*Sumner, C.J., O'Mard, L.P., Lopez-Poveda, E.A., and Meddis, R. (2002b). "A revised model of the inner-hair cell and auditory nerve complex," *J. Acoust. soc.Am.* 111, 2178-2189.
- \*Viemeister, N.F., Shivapuja,G. and Recio, A. (1992). "Physiological correlates of temporal integration," In: Cazals, Y, Horner, K. and Demany, L. *Auditory Physiology and Perception*, Pergamon Press, Oxford, pp 323-329.
- \*Wiegrebe, L. and Meddis, R. (2004) 'The representation of periodic sounds in simulated sustained chopper units of the ventral cochlear nucleus' *Journal of the Acoustical Society of America*, 115, 1207-1218
- \*Winter, I. M., Robertson, D., and Yates, G. K. (1990). "Diversity of characteristic frequency rate-intensity functions in guinea pig auditory nerve fibers," *Hear. Res.* 45, 191–202.

## Appendix 1. Computational details.

The model is for guinea pig and consists of a cascade of stages. All units are international units. The model was evaluated once every 1e-5 sec.

### A. Middle-ear filtering

A cascade of Two linear band-pass Butterworth filters were used to model the response of the **guinea pig** middle ear. The first filter is second order with an upper cut-off of 25kHz and a lower- cut-off of 4kHz. The second filter is third order with upper- and lower- cut-offs of 30kHz and 700Hz. Both have unity gain in the passband. The output velocity,  $x(t)$ , is found after applying a scalar of  $1.4e-4 \text{ m s}^{-1} \text{ Pa}^{-1}$

### B. Mechanical filtering: DRNL filter

The filtering of the BM is modeled with a ‘Dual-Resonance-Non-Linear’ (DRNL) filter architecture that has been described and evaluated more fully elsewhere (Meddis *et. al.*, 2001; Lopez-Poveda and Meddis, 2001; Sumner *et al.*, 2003b). The input is stapes velocity,  $x(t)$ . The DRNL filter consists of two parallel pathways, one linear and the other non-linear, whose outputs are summed to produce an output,  $v(t)$  representing the velocity of the cochlear partition in  $\text{ms}^{-1}$ .

The *nonlinear* pathway consists of three identical first-order gammatone filters; a compression function followed by three more identical gammatone filters and then by four first-order Butterworth low passes filters. The compression in the non-linear pathway is described by:

$$v_t = \text{SIGN}(x_t) \times \text{MIN}(a/|x_t|, b/|x_t|^v) \quad (1)$$

where  $a$  and,  $b$  are parameters specific to a particular BM location. The compression exponent,  $v$ , was 0.1.

The *linear* path consists of a gain function followed by a cascade of three identical gammatone filters followed by a cascade of four Butterworth low pass filters. For both paths the cut-off frequency of the low pass filters was set to the CF of the corresponding gammatone filters.

The CF of the nonlinear path gammatone filters ( $CF_{NL}$ ) is set to the desired BF of the filter as a whole, i.e. as a function of its location along the cochlear partition. The other parameters of the system are set relative to  $CF_{NL}$  using the formula:

$$\log(\text{parameter}) = p_0 + m \log(CF_{NL}) \quad (2)$$

Table 1 shows the parameters  $p_0$  and  $m$  values required to compute the parameters  $a$ ,  $b$ , the bandwidths of the component gammatone filters in linear ( $BW_{lin}$ ) and nonlinear ( $BW_{NL}$ ) pathways, the gain of the linear filter ( $G_{lin}$ ), and the centre frequency of the linear filter ( $CF_{lin}$ ).

$\log(\text{parameter}) = p_0 + m \log(CF_{NL})$	$p_0$	$M$
Bandwidth of non-linear path, $BW_{NL}$ (Hz).	0.8	0.58
Compression parameter, $a$	1.87	0.45
Compression parameter, $b$	-5.65	0.875
Center Frequency of linear path, $CF_{lin}$ (Hz).	0.339	0.895
Bandwidth of linear path, $BW_{lin}$ (Hz).	1.3	0.53
Linear path gain, $G_{lin}$ .	5.68	-0.97

**Table A1. Coefficients for computing parameters of the guinea pig DRNL filters as a function of  $CF_{NL}$ .**

### C. IHC receptor potential

	Sumner et al (2002)
$E_t$ , endocochlear potential (V)	100e-3
$E_k$ , potassium reversal potential (V)	-70.45e-3
$G_0$ , resting conductance (S= Siemens)	1.974e-9
$G_k$ , potassium conductance (S)	18e-9
$E_k$ correction, $R_p/(R_t+R_p)$	0.04
$G_{cilia}^{max}$ , max. mechanical conductance (S)	8e-9
$s_0$ , displacement sensitivity ( $m^{-1}$ )	85e-9
$u_0$ , displacement offset (m)	7e-9
$s_1$ , displacement sensitivity ( $m^{-1}$ )	5e-9
$u_1$ , displacement offset (m)	7e-9
$C_m$ , total capacitance (F)	6e-12
$\tau_c$ cilia/BM time constant (s).	2.13e-3
$C_{cilia}$ , cilia/BM coupling gain (dB)	16

**Table A2 IHC receptor potential. Values are taken from Sumner et al., 2002b, Table I.**

Note that  $s_1$  was originally given incorrectly as 5e-7.

The guinea pig model hair cell parameters are taken from Sumner *et al.*. 2002, 2003a, 2003b). The displacement of the IHC cilia,  $u(t)$ , as a function of BM velocity,  $v(t)$ , is given by

$$\tau_c \frac{du(t)}{dt} + u(t) = \tau_c C_{cilia} v(t) \quad (3)$$

where  $C_{cilia}$  is a gain factor and  $\tau_c$  is a time constant. The cilia displacement causes a change in the in the apical conductance  $G(u)$ . The total apical conductance is given by:

$$G(u) = G_{cilia}^{max} \left[ 1 + \exp\left(-\frac{u(t) - u_0}{s_0}\right) \right] \left[ 1 + \exp\left(-\frac{u(t) - u_1}{s_1}\right) \right]^{-1} + G_a \quad (4)$$

where  $G_{cilia}^{max}$  is the transduction conductance with all channels open, and  $G_a$  is the passive conductance in the apical membrane.  $s_0, u_0, s_1$  and  $u_1$  are constants determining the exact shape of the non-linearity.  $G_a$  is computed as

$$G_a = G_0 - G_{cilia}^{max} \left[ 1 + \exp\left(\frac{u_0}{s_0}\right) \left[ 1 + \exp\left(\frac{u_1}{s_1}\right) \right] \right]^{-1}$$

where  $G_0$  is the resting conductance

Needs checking! This is nonsense

The membrane potential of the cell body is modeled with a passive electrical circuit analog:

$$C_m \frac{dV(t)}{dt} + G(u)(V(t) - E_t) + G_k(V(t) - E_k') = 0 \quad (5)$$

where  $V(t)$  is the intracellular hair cell potential;  $C_m$  is the cell capacitance;  $G_k$  is the voltage-invariant basolateral membrane conductance;  $E_t$  is the endocochlear potential; and  $E_k' = E_k + E_t R_p / (R_t + R_p)$  is the reversal potential of the basal current  $E_k$  corrected for the resistance ( $R_t, R_p$ ) of the supporting cells.

#### **D. Calcium controlled transmitter release function**

Depolarisation of the IHC membrane leads to an increase in the Calcium current ( $I_{Ca}$ ):

$$I_{Ca}(t) = G_{Ca}^{max} m_{I_{Ca}}^3(t) (V(t) - E_{Ca}) \quad (6)$$

where  $E_{Ca}$  is the reversal potential for calcium and  $G_{Ca}^{max}$  is the calcium conductance in the vicinity of the synapse, with all the channels open.  $m_{I_{Ca}}(t)$  is the fraction of calcium channels that are open. Its steady state value,  $m_{I_{Ca},\infty}$  is modeled by a Boltzmann function,

$$m_{I_{Ca},\infty} = \left[ 1 + \beta_{Ca}^{-1} \exp(-\gamma_{Ca} V(t)) \right]^{-1} \quad (7)$$

where  $\beta_{Ca}$  and  $\gamma_{Ca}$  are constants chosen to reflect published observations of calcium currents (see Table II), and  $m_{I_{Ca}}(t)$  is a low pass filtered function of  $m_{I_{Ca},\infty}$

$$\tau_m \frac{dm_{I_{Ca}}(t)}{dt} + m_{I_{Ca}}(t) = m_{I_{Ca},\infty} \quad (8)$$

where  $\tau_m$  is a calcium current time constant.

Pre-synaptic calcium concentration  $[Ca^{2+}](t)$  is modeled as a first-order low-pass filtered function of calcium current,  $I_{Ca}(t)$

original published model (Sumner model):

$$\frac{d[Ca^{2+}](t)}{dt} = [I_{Ca}(t) - [Ca^{2+}](t)] / \tau_{[Ca]} \quad (9)$$

new model (calcium clearance model)

$$\frac{d[Ca^{2+}](t)}{dt} = I_{Ca}(t) - [Ca^{2+}](t) / \tau_{[Ca]} \quad (10)$$

where  $\tau_{[Ca]}$  is a time constant.

The probability of the release of transmitter is proportional to the cube of  $Ca^{2+}$  concentration:

original published model (Sumner model):

$$k(t) = \max([Ca^{2+}]^3(t) - [Ca^{2+}]_{thr}^3, 0) \quad (11)$$

new model (calcium clearance model)

$$k(t) = z([Ca^{2+}]^3(t)) \quad (12)$$

where  $[Ca^{2+}]_{thr}$  is a threshold constant,  $z$  is a scalar for converting calcium levels into release rate.

	<i>Sumner et al.</i>	<i>calcium clearance</i>
$E_{Ca}$ , reversal potential (V)	0.066	0.066
$\beta_{Ca}$	400	400
$\gamma_{Ca}$	130	130
$\tau_m$ , calcium current time constant (s)	1e-4	1e-4
$\tau_{Ca}$ , calcium clearance time constant (s)		
HSR	1e-4	3.5e-4
MSR	1e-4	1.5e-4
LSR	1e-4	0.75e-4
$z$ , scalar converts from $[Ca^{2+}]^3$ to probability	20e31	1e56
$G_{Ca}^{max}$ , max. $Ca^{2+}$ conductance		8e-9 (S)
HSR	7.2e-9	
MSR	2e-9	
LSR	1.6e-9	
$[Ca^{2+}]_{thr}$ , threshold		Not used
HSR	0	
MSR	3.3e-14	
LSR	1.4e-11	

**Table 1 Parameters for control of pre-synaptic calcium levels.**

### E. Quantal and probabilistic model of synaptic adaptation

More detailed accounts of this process in a probabilistic form can be found in Meddis (1986, 1988) and Hewitt and Meddis (1991) and Sumner (2002 a and b). A description of the quantal version is found in Sumner (2003).

Individual vesicles of neurotransmitter (probably glutamate), are released from an *immediate pre-synaptic* ( $q$ ) store into the *cleft* ( $c$ ), at a rate,  $k(t)$ , that is dependent on calcium concentration. In the cleft, the transmitter disperses and some is lost from the system at a rate  $l$ . The remaining transmitter in the cleft is taken back into the cell into a *reprocessing* ( $w$ ) store at a rate  $r$ . Here it is repackaged into vesicles that are returned to the immediate store at a rate  $x$ . Additionally,  $q$  is continuously replenished with new transmitter vesicles at a rate,  $y[M-q(t)]$  where  $M$  represents the maximum number of transmitter quanta that can be held in the immediate store ( $q$ ).

Neurotransmitter in the immediate store is quantal, and enters and leaves the immediate store stochastically. The stochastic transport of neurotransmitter is described by the function  $N(n, \rho)$ , in which each of  $n$  quanta has an equal probability of release,  $\rho dt$ , in a single simulation epoch. In the cleft and reprocessing stores, transmitter is a continuous quantity. This means, for instance, that the contents of the reprocessing store must be an integer number greater than or equal to one for a transmitter quantum to be eligible to re-join the immediate store. The output from the synapse is a stream of discrete events indicating vesicle releases,  $N(q(t), k(t))$ .

$$\frac{dq(t)}{dt} = N(w(t), x) + N([M - q(t)] y) - N(q(t), k(t)) \quad (13)$$

$$\frac{dc(t)}{dt} = N(q(t), k(t)) - lc(t) - rc(t) \quad (14)$$

$$\frac{dw(t)}{dt} = rc(t) - N(w(t), x) \quad (15)$$

parameter	value
y, replenishment rate ( $s^{-1}$ )	<b>3</b>
l, loss rate ( $s^{-1}$ )	2580
x, reprocessing rate ( $s^{-1}$ )	<b>30</b>
r, recovery rate ( $s^{-1}$ )	6580
M, max. free transmitter quanta	10
Sumner (LSR only)	(8)

**Table A3. IHC transmitter release parameters. These values were published in Meddis and O'Mard (2005) and optimised using recovery from forward masking data.**

Initial values for the variable quantities are found as follows (Meddis *et al.*, 1990):

$$c(0) = k(0) * y * m / (y * (1+r) + k(0) * 1) \quad (16)$$

$$q(0) = c(0) * (1+r) / k(0) \quad (17)$$

$$w(0) = c(0) * r / x \quad (18)$$

### **F. Auditory nerve response**

A absolute refractory effect lasting 0.75 ms was applied. Thereafter, a release event was converted into a spike on a probabilistic basis as a function of time (s) since the last spike:

$$P_{\text{conversion}} = 1 - \exp(-t/0.0006) \quad (19)$$

Each spike is treated as a pulse one epoch wide and added to a PSTH with a 0.0005s bin width.

### **G. Sustained chopper model**

This model is based on MacGregor's (1987) point neuron model. It consists of two stages; input at the dendrites and spike generation at the soma. The original MacGregor neuron provides for the possibility that the threshold can vary This has been omitted here. In AMS this is achieved by setting  $c=0$ .

The input to the dendrites is a PSTH with 0.0005s wide bins. The dendritic input stage applies a first-order low pass filter (3 dB cut-off at 200 Hz) to the PSTH to produce a representation of input current,  $I(t)$  to the soma.

This is then scaled by a factor of 1/number of input fibers (1/20 in this example).

The trans-membrane potential at the soma is represented as a deviation from resting potential,  $E_r$ , and tracked using the equation:

$$dE(t)/dt = (-E(t) + \{[I(t)/G] + G_k(t)/G[E_k - E(t)]\})/\tau_m \quad (20)$$

where  $\tau_m$  is the membrane time constant,  $E_k$  is the potassium reversal potential (relative to  $E_r$ ) and  $G_k(t)$  is the cell potassium conductance:

$$dG_k(t)/dt = [-G_k(t) + (b \cdot s)]/\tau_{Gk} \quad (21)$$

where  $\tau_{Gk}$  is the potassium time constant,  $b$  is the increase in  $G_k$  following an AP indicated when  $s=1$ . An AP is initiated when the membrane potential exceeds a threshold  $E(t) > Th_0$ . The threshold was fixed throughout.

Membrane time constant $\tau_m$ (s)	0.001
Potassium recovery time constant $\tau_{Gk}$ (s)	0.0002
Increment in $G_k$ on firing $b$	0.01
Resting threshold $Th_0$ (mV)	1.6
Potassium reversal potential $E_k$ (mV)	-10

**Table A4. MacGregor point neuron parameters (Wiegube and Meddis 2004)**

## Footnotes

---

- <sup>1</sup> DSAM: Development software for Auditory Modelling, a library of compiled C-code routines for auditory modelling. AMS: auditory modelling system., an application for creating running and displaying complex auditory models using DSAM routines. This software is available from the authors.